AIChE

Numerical Investigations on the Development of Plate Reformers: Comparison of Different Assignments of the Chambers

Qi Zhang and Xuedong Zhu
Dept. of Chemical Engineering, East China University of Science and Technology, Shanghai 200237, China

Hideo Kameyama
Dept. of Chemical Engineering, Faculty of Engineering, Tokyo University of Agriculture and Technology, Tokyo 184-8588, Japan

DOI 10.1002/aic.11592
Published online September 5, 2008 in Wiley InterScience (www.interscience.wiley.com).

Two compact plate methane steam reformers, consisting of closely spaced plate electrically heated alumite catalysts, have been numerically investigated in the relation to heat and mass transfer. Based on the ordinary heat exchange reformer (HER), where endothermic and exothermic reactions take place in alternative chambers, a developed heat exchange reformer coupled with preheating chamber (PHER) is proposed by integrating a preheating chamber with a combustion chamber. The simulation results predicted that the PHER could be started by electrical heating through a catalyst at the beginning, even with the inlet combustion gas temperature of 298 K, whereas the HER requires a combustion inlet temperature as high as 723 K, which showed the PEHR high potential for simplifying the heat exchange network in a fuel processor. On the other hand, the compact structure of the reformer could constitute a single unite of reformer, which is easy to be placed and scaled up. © 2008 American Institute of Chemical Engineers *AIChE J,* 54: 2707–2716, 2008
Keywords: methane steam reformer, methane combustion, electrically heated alumite catalyst, simulation

Introduction

The application of fuel cell technology for an efficient, decentralized supply of electrical energy and which is friendly to the environment is widely studied. For the 0.25–1 kW class residential fuel cell system, the methane steam reforming is regarded as a major route for the generation of H_2 rich gas for the accompanying fuel stack.[1,2] Various reviews of steam reformers have discussed the conventional process, which is based on Ni catalysts in multitubular reactors operated at temperatures varying from 773 K (inlet) to 1073 K (outlet), pressures ranging from 20 to 40 bar, and S/C (Steam to Carbon ratio) in the feed from 2 to 4.[3,4] However, this process suffers from a number of limitations, such as diffusion and thermodynamic limitation, great pressure drop and large size. Furthermore, for residential utilization, start-up time presents one of the problems that affect the performance of the fuel cell, where the reformer plays an important role in shortening the start-up time.[1,5]

To deal with the above problems, structured catalytic reactors have been extensively investigated. The plate catalysts were reported in various preparation methods, such as a plasma method of active metal powder on a metal carrier,

Correspondence concerning this article should be addressed to Q. Zhang at doraqi@hotmail.com and X. Zhu at xdzhu@ecust.edu.cn.

pressing an active phase on a heat-conducting carrier.[6,7] Especially, the anodization technology of the Al plate to reform a more constructive catalyst carrier was reported in reaction systems such as volatile organic compound combustion and selective catalytic reduction of NO_x, etc.[8,9] However, the Al_2O_3/Al catalyst carrier cannot withstand a high reaction temperature above 823 K. Therefore, a novel structured catalyst, that is, the electrically heated alumite catalyst (EHAC) was proposed. The catalyst carrier was also obtained by anodization technology of Al/alloy/Al plate.[10] Because of the existence of the alloy layer, the catalyst could be electrically heated, which was promising for a prompt heat supply. Meanwhile, the results of thermal endurance test at 1073 K showed the catalyst had a high thermal resistance, and no Al_2O_3 layer was found to shell from the alloy layer because the alumina film is derived form the Al layer.[11] Owing to its advantages mentioned earlier, the EHAC was applied in a plate wall methane steam reformer.

As methane steam reforming is a substantial endothermic reaction, a heat source is necessary. From a viewpoint different from that of a conventional fixed-bed reactor, heat exchange reactor by utilizing the high heat transfer performance of the plate wall reactor was proposed by Hunter and McGuire.[12] With this setup it is possible to make exothermic and endothermic reactions that proceed simultaneously in one reactor to use the generated heat from the exothermic reaction as heat source for the endothermic reaction or to use the endothermic reaction to control the thermal energy generated by the exothermic reaction. The approach shares a similar mechanism with that of the heat exchange equipment, which is often found in large-scale processes, such as hydrocarbon cracking, steam reforming, and dehydrogenation. Reay[13] explained the benefits of such approach in the context of the catalytic plate reactor, which is comprised of closely spaced catalytically coated metal plates, so that it proceeds at lower temperatures which pose fewer constraints for the materials of the reactor.

For design of the reactor, the simulation technology is an important tool to accumulate the optimization conditions of design parameters and to predict reactor performance in various operation situations. The heat exchange reformers (HERs) have also been numerically developed, where the methane reforming chamber was coupled with combustion chambers on the upper and lower sides.[4,10,14] However, all of these designs are based on the combustion inlet gas at a rather high temperature, as it is difficult to induce methane combustion at a low temperature. Since the heat exchange system affects the factors of the whole fuel cell system's optimization, such as the cost, volume, etc., based on the reported HER, a more compact reformer has been proposed in this article, which consists of a reforming chamber, combustion chamber, and preheating chamber of the combustion gas, by heat recovery. At the beginning of the reformer's operation, the catalysts are electrified to ignite the combustion reaction and sequentially to start the reforming reactions. The combustion heat is also designed to supply the heat to warm up the cold inlet combustion reactants to increase the heat exchanger efficiency.

In this study, a dynamic multiple-phase 2-D model was developed to accumulate relevant information before designing the reformer. Compared with an ordinary HER, the heat and mass transfer performance of the developed reformer was discussed as affected by the inlet temperature, the electrically heating operation, the chamber height, and the fuel ratio on the performance of the reformers. Meanwhile, a simplified heat exchange network of the fuel processor was also proposed using the newly developed reformer.

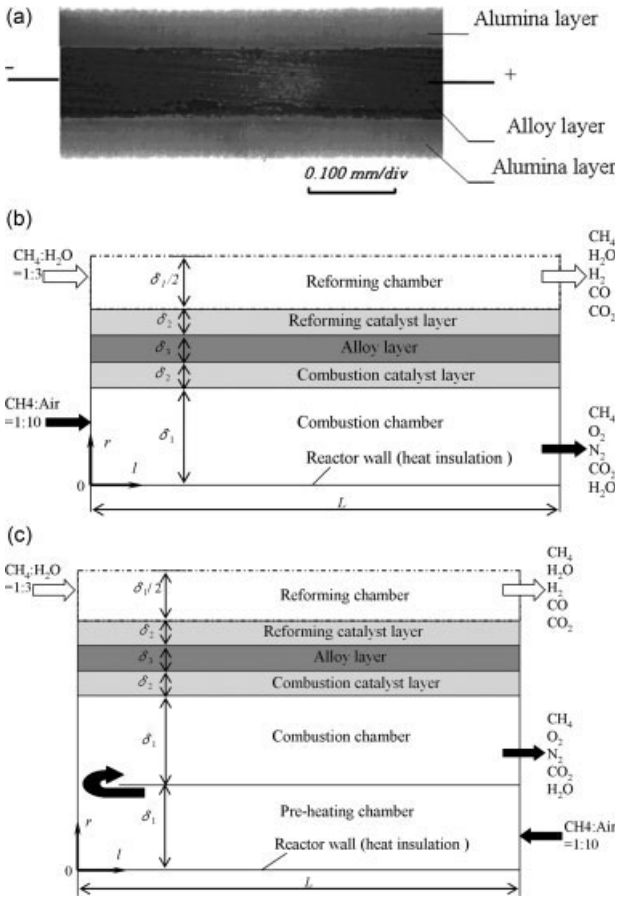

Figure 1. (a) Cross section photo of the EHAC; (b) Heat exchange reformer (HER); (c) Heat exchange reformer coupled with preheating chamber (PHER).

(For clarity, the schemes are not drawn in a real scale).

Model development

Reformer Design. For the plate wall reformers, high thermal conductivity EHAC was applied. Figure 1a shows the cross section of obtained Al_2O_3/alloy catalyst by anodization technology. The generic HERs' configurations are schematically illustrated in Figures 1b, c. For the ordinary HER, that is, HER, it consists of the combustion chambers and the reforming chamber. The upper and lower chambers are methane combustion and the middle channel involves methane reforming. A thin plate catalyst with different catalyst supporting separates the combustion chamber from the reforming chamber. According to the symmetry of conditions at the centerline of the reactor, half of the reactor, as shown in Fig-

Table 1. Conditions for Two Kind Reformers

	EHR	PHER
Reactor		
Length: L (m)	0.15	
Chamber height: δ_1 (m)	0.005	
Initial temperature	298 K in the reformer (cold start)	
Inlet condition		
Mole fraction	S/C = 3 (reforming side) CH_4/Air = 1/10 (combustion side)	
Temperature (K)	723	523 (reforming side) 298 (combustion side)
CH_4 flow rate (mol s^{-1})	8.93×10^{-4} (reforming side) 1.30×10^{-4} (combustion side)	
Pressure (Kpa)	101.3	
EHAC		
Thickness ($\times 10^{-6}$ m)		
Alumina layer: δ_2	40	
Alloy layer: δ_3	50	
Metal loading	Ni 13 (wt %) Pt 0.14 (wt %)	
Electrical resistance (Ω)	0.2	
Electrical current (A)	8 ~ 15	

ure 1b, has been discussed in the models. Figure 1c shows the structure of the HER with preheating chamber, that is, heat exchange reformer coupled with preheating chamber (PHER), which consists of the reforming chamber, combustion chamber, and preheating chamber of the combustion gas. The gas conducted into the preheating chamber is preheated by the exothermic reaction heat in the combustion chamber by means of direct heat transfer. In this work, we simulated a reformer with the capability to provide enough H_2 for a 250 W domestic fuel cell. In the case of the steam to carbon ratio (S/C) = 3, assuming the conversion of methane steam reforming of 98% and fuel utilization rate of 70%. The conditions used in the simulation in the base case are shown in Table 1. In the following sections, the calculation conditions are in accordance with those of the base case unless otherwise stated.

Kinetics

The reaction kinetics for methane steam reforming and combustion were derived from our experimental results. In this work, Ni was selected as the active metal for the methane reforming reactions and Pt for the methane combustion reaction. The kinetic characteristics for reforming were obtained using a differential reactor, avoiding concentration and temperature gradients by adopting the kinetic mechanism cited by Zhang et al. and Numaguchi and Kikuchi.[10,15] The partial pressure of each reactant can be calculated as the product of its local mole fraction and the total pressure. For the catalytic combustion using a Pt catalyst, the order in methane is usually about unity, whereas the reaction order in oxygen tends toward zero.[4,16] In this simulation, a first-order kinetic expression with respect to methane was utilized in the calculation. The reaction rate equations are shown as follows:

$$CH4 + H_2O \rightarrow CO + 3H_2 \quad (\Delta H)_1 = 2.27 \times 10^5 \text{ J mol}^{-1}$$

$$CO + H_2O \rightarrow CO_2 + H_2 \quad (\Delta H)_2 = -3.32 \times 10^4 \text{ J mol}^{-1}$$

$$CH_4 + 2O_2 \rightarrow CO_2 + 2H_2O \quad (\Delta H)_3 = -8.17 \times 10^5 \text{ J mol}^{-1}$$

$$w_1 = k_1 \frac{P_{CH_4} - P_{CO}P_{H_2}^3/(K_1 P_{H_2O})}{P_{H_2O}^{0.6}} \tag{1}$$

$$w_2 = \frac{k_2[P_{CO} - (P_{CO_2}P_{H_2})/(K_2 P_{H_2O})]}{P_{H_2O}^{0.55}} \tag{2}$$

$$w_3 = k_3 P_{CH_4} \tag{3}$$

where

$$k_1 = 1.14 \times 10^9 \exp[-163000/(R_g T)] (\text{mol Pa}^{-0.40}\ \text{kg}_{\text{cat}}{}^{-1}\ \text{s}^{-1})$$

$$k_2 = 18.7 \times \exp[-66000/(R_g T)]\ (\text{mol Pa}^{-0.45}\ \text{kg}_{\text{cat}}{}^{-1}\text{s}^{-1})$$

$$k_3 = 4 \times 10^8 \times \exp[-833000/(R_g T)]\ (\text{mol Pa}^{-1}\ \text{kg}_{\text{cat}}{}^{-1}\text{s}^{-1})$$

$$K_1 = \exp(-22430/T + 26.078) \quad (\text{Pa}^2)$$

$$K_2 = \exp(4400/T - 4.036)$$

The reaction rates for the formation of CO and CO_2 and the disappearance of methane and steam in the reforming chamber are obtained from Eqs. 4–7:

$$\text{For } CH_4 \text{ disappearance rate}: \ w_{1,1} = -w_1 \tag{4}$$

$$\text{For } H_2O \text{ disappearance rate}: \ w_{2,1} = -(w_1 + w_2) \tag{5}$$

$$\text{For CO formation rate}: w_{3,1} = w_1 - w_2 \tag{6}$$

$$\text{For } CO_2 \text{ formation rate}: \ w_{4,1} = w_2 \tag{7}$$

Meanwhile, the reaction rates for the formation of H_2O and CO_2 and for the disappearance of methane and oxygen in the combustion chamber can also be obtained from Eqs. 8–11:

$$\text{For } CH_4 \text{ disappearance rate}: \ w_{1,2} = -w_3 \tag{8}$$

$$\text{For } O_2 \text{ disappearance rate}: \ w_{2,2} = -2w_3 \tag{9}$$

$$\text{For } CO_2 \text{ formation rate}: \ w_{3,2} = w_3 \tag{10}$$

$$\text{For } H_2O \text{ formation rate}: \ w_{4,2} = 2w_3 \tag{11}$$

The heat of reaction, $(\Delta H)_m$ (m = 1, 2, 3), was determined at 1160 K. The equilibrium constant, K_m (m = 1, 2), was estimated from thermodynamic data.

Model development

The following assumptions were made:

(1) The gases are assumed as ideal gasses and as suitable for the ideal gas law to apply to; (2) The chemical reactions take place only on the catalyst layer; (3) The pressure drop is neglected in all runs; (4) Heat loss of the reformer is neglected; (5) The heat radiation is neglected.

The numerical model in this study derived from the previously reported coaxial model and plate heat exchange

model.[10,17] Considering the structure of the reformers, five different domains were identified: a reforming chamber, a catalyst layer for reforming, an alloy layer, a catalyst layer for combustion, and a combustion chamber integrated with a preheating chamber. The partial differential equations (PDEs) are given in Table 2. The dependence of the physical properties of chemical species on temperature is also shown in the table.[4,18,19] The heat capacities of the spices were obtained from the software of MiniMalt. The diffusion coefficients has been calculated for a binary mixture i and steam (reforming chamber) or air (combustion chamber). Table 3 shows the boundary conditions of the model, where the catalyst surfaces and alloy surfaces are regarded as the interior boundaries. The boundary conditions involve at the inlet specified (Dirichlet) conditions. An insulated wall and no flux conditions at the outlet for the HER and PHER are also presented in the table.

The PDEs were solved using FEMLAB, a PDE solver tool from COMSOL, which is especially designed for the multiphysics problems, that is, systems that consist of coupled phenomena described by different models using the proven finite element method. The software runs the finite element analysis together with adaptive meshing and error control using a variety of numerical solvers (Comsol, 2005).[20] We used quadratic rectangular elements and a nonuniform mesh, with small elements located at the gas–solid interface and solid phase. Because of the implicit nature of the scheme and the nonlinear nature of the governing equations, the time dependent solver was chosen to solve the PDEs. The time-dependent solver uses variable-order variable-step-size backward differentiation formulas to generate a linear system at previous time step to achieve the solution with good stability at the current time.

Table 2. Model Equations

Model Equations
Gas phase
Mass transfer
$\frac{\partial y_{i,j}}{\partial t} + u_j \frac{\partial y_{i,j}}{\partial l} = \frac{\partial}{\partial r}(D_{i,j} \frac{\partial y_{i,j}}{\partial r}) + \frac{\partial}{\partial l}(D_{i,j} \frac{\partial y_{i,j}}{\partial l})$
Heat transfer
$\bar{\rho}_j \mathrm{Cp}_j \frac{\partial T_j^g}{\partial t} + u_j \cdot \bar{\rho}_j \cdot \mathrm{Cp}_j \frac{\partial T_j^g}{\partial l} = \frac{\partial}{\partial r}(\lambda_{\mathrm{er},j} \frac{\partial T_j^g}{\partial r}) + \frac{\partial}{\partial l}(\lambda_{\mathrm{er},j} \frac{\partial T_j^g}{\partial l})$
Navier-Stokes velocity equation
$\bar{\rho}_j \frac{\partial u_{r,j}}{\partial t} + \bar{\rho}_j (\frac{\partial u_{r,j}^2}{\partial r} + \frac{\partial u_{r,j} u_{l,j}}{\partial l}) = \mu_j (\frac{\partial^2 u_{r,j}}{\partial r^2} + \frac{\partial^2 u_{l,j}}{\partial l^2})$
$\bar{\rho}_j \frac{\partial u_{l,j}}{\partial t} + \bar{\rho}_j (\frac{\partial u_{l,j}^2}{\partial l} + \frac{\partial u_{r,j} u_{l,j}}{\partial r}) = \mu_j (\frac{\partial^2 u_{r,j}}{\partial r^2} + \frac{\partial^2 u_{l,j}}{\partial l^2})$
Continuity equation
$\frac{\partial u_{r,j}}{\partial r} + \frac{\partial u_{l,j}}{\partial l} = 0$
$\overline{\rho}_j \frac{\partial y_{i,j}}{\partial t} + \frac{\partial}{\partial r}(\overline{\rho}_j D_{\mathrm{eff}_{i,j}} \frac{\partial y_{i,j}}{\partial r}) = w_{i,j} M_{i,j} \rho_{\mathrm{cat}}$
Heat transfer
$C\mathrm{p}^{\mathrm{cat}} \overline{\rho}_j \frac{\partial T_j^{\mathrm{cat}}}{\partial t} + \frac{\partial}{\partial r}(\lambda_{\mathrm{er},j} \frac{\partial T_j^{\mathrm{cat}}}{\partial r}) + \frac{\partial}{\partial l}(\lambda_{\mathrm{er},j} \frac{\partial T_j^{\mathrm{cat}}}{\partial l}) = H_{i,j} w_{i,j} \rho_{\mathrm{cat}}$
Alloy layer
In case of nonheat input
$C\mathrm{p}^{\mathrm{alloy}} \overline{\rho}_j \frac{\partial T^{\mathrm{alloy}}}{\partial t} + \lambda^{\mathrm{alloy}} [\frac{\partial}{\partial l}(\frac{\partial T^{\mathrm{alloy}}}{\partial l}) + \frac{\partial}{\partial r}(\frac{\partial T^{\mathrm{alloy}}}{\partial r})] = 0$
In case of electrical heating
$C\mathrm{p}^{\mathrm{alloy}} \overline{\rho}_j \frac{\partial T^{\mathrm{alloy}}}{\partial t} + \lambda^{\mathrm{alloy}} [\frac{\partial}{\partial l}(\frac{\partial T^{\mathrm{alloy}}}{\partial l}) + \frac{\partial}{\partial r}(\frac{\partial T^{\mathrm{alloy}}}{\partial r})] = P_{\mathrm{ele}}$
No mass transfer $\forall r, \forall l \quad y_{i,j} = 0$
Properties
$\mu_j = \sum_i y_i \mu_i \quad C_{pj} = \sum_i y_i C_{pi} \quad \lambda_{\mathrm{er},j} = \sum_i y_i \lambda_i$
$D_i = D_{i,0} (\frac{T}{T_0})^{1.75}$
$D_{\mathrm{eff},i} = \frac{\varepsilon}{\tau} \left[(97 \cdot R\mathrm{p} \sqrt{\frac{T}{M_{i,j}}})^{-1} + \frac{1}{D_i} \right]^{-1}$

Table 3. Boundary Conditions of the Model

Boundary conditions
Internal boundaries
$\forall l, r =$ catalyst surface
$\rho_j D_{ri,j} \frac{\partial y_{i,j}^g}{\partial r} = -\rho_j D_{\mathrm{eff}_{i,j}} \frac{\partial y_{i,j}^g}{\partial r} \quad \lambda_{\mathrm{er}_j}^{\mathrm{g}} \frac{\partial T_j^g}{\partial r} = \lambda_{\mathrm{er}_j}^{\mathrm{cat}} \frac{\partial T_j^{\mathrm{cat}}}{\partial r}$
$\forall l, r =$ alloy surface
$\frac{\partial y^{\mathrm{cat}}}{\partial r} = \frac{\partial y^{\mathrm{alloy}}}{\partial r} = 0 \quad \lambda_{\mathrm{er}_j}^{\mathrm{cat}} \frac{\partial T_j^{\mathrm{cat}}}{\partial r} = \lambda_{\mathrm{er}_j}^{\mathrm{alloy}} \frac{\partial T_j^{\mathrm{alloy}}}{\partial r}$
$\forall l, r =$ alloy surface between the preheating and combustion chambers
$\frac{\partial y^g}{\partial r} = 0 \quad \lambda_{\mathrm{er}_j}^{g} \frac{\partial T_j^g}{\partial r} = \lambda_{\mathrm{er}_j}^{\mathrm{alloy}} \frac{\partial T_j^{\mathrm{alloy}}}{\partial r}$
Inlet conditions
For the HER $\forall r, l = 0 \quad y_{i,j} = y_{i,j}^0 \quad T_j = T_{\mathrm{in}}$
For the PHER $r \in [0, \delta_1], l = L \quad y_{i,2} = y_{i,2}^0 \quad T_j = T_{\mathrm{in}}$
$r \in [0, 2\delta_1 + 2\delta_2 + \delta_3], l = L \quad y_{i,1} = y_{i,1}^0 \quad T_j = T_{\mathrm{in}}$
Center conditions
For the HER, $\forall l, \quad r = 1.5\delta_1 + 2\delta_2 + \delta_3$
For the PHER $\forall l, \; r = 2.5\delta_1 + 2\delta_2 + \delta_3$
(Central line of the reforming channel)
$\frac{\partial T_{j=1}}{\partial l} = 0$
$\frac{\partial y_{i,j=1}}{\partial l} = 0$
Reactor wall conditions $\forall l, \quad r = 0$
$\frac{\partial T_{j=2}}{\partial l} = 0$
$\frac{\partial y_{i,j=2}}{\partial l} = 0$
Initial conditions $\forall r, l, \; t = 0$
Cold environment $T\|_{t=0} = 298\,\mathrm{K} \quad y_{i,j}\|_{t=0} = 0$

Results and Discussion

Steady-state performance of the reformers

In this work, the steady-state heat transfer performance of the reformers was compared first. The simulation results show that when the reaction time is long enough, such as 120 min, the temperature and concentration distribution keep consistent, and the reaction performance can be regarded as a steady state. Figure 2 shows the profiles of the temperature in the combustion chamber and CH_4 conversion in the reforming chamber for the HER at different inlet temperatures. For the HER, reforming inlet temperatures were set as the same as that of the combustion side. A hot spot is found near the inlet of the reformer due to CH_4 combustion being a fast exothermic oxidation reaction, heat generation overcomes heat consumption, and both streams are heated up. The rise in temperature accelerates the endothermic reaction, which in turn results to an increase of heat consumption so that eventually the temperature drops. It can be seen, that when T_{in} is as low as 673 K, it will take a half of the reformer length for the gas temperature to reach a reasonable ignition point. As a result, the CH_4 reforming conversion shows a distinctive decrease when the inlet temperature is set as 673 K. As methane combustion's ignite temperature is as high as 723 K, the lower inlet temperature has difficulty to activate the reaction system promptly, which is the reason that various studies set the methane combustion inlet temperature at a rather high temperature in simulations or operations. Further, the transverse temperatures difference between the reforming and combustion chamber is explicated in Fig-

ure 2c when T_{in} is set as 723 K. The transverse temperature difference at position l is calculated as:

$$\Delta T|_l = \bar{T}_{comb}|_l - \bar{T}_{ref}|_l \quad (12)$$

where $\bar{T}_{comb}|_l$ means the average temperature in the combustion chamber in r direction and $\bar{T}_{ref}|_l$ means that in the reforming chamber. It can be seen that the gas temperature

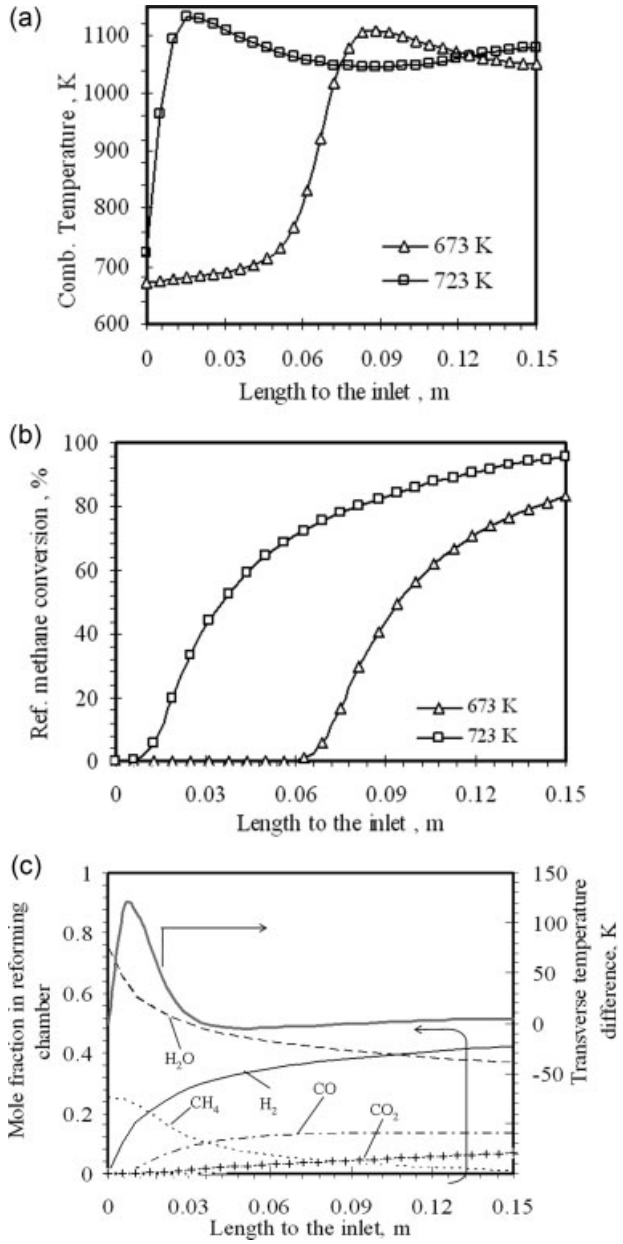

Figure 2. The profiles of HER for (a) the temperature in the combustion chamber with different inlet temperature and (b) methane steam conversion in the reforming chamber, (c) mole fraction and transverse temperature difference profiles in the reforming channel along the reformer length with inlet temperature of 723 K at t = 120 min.

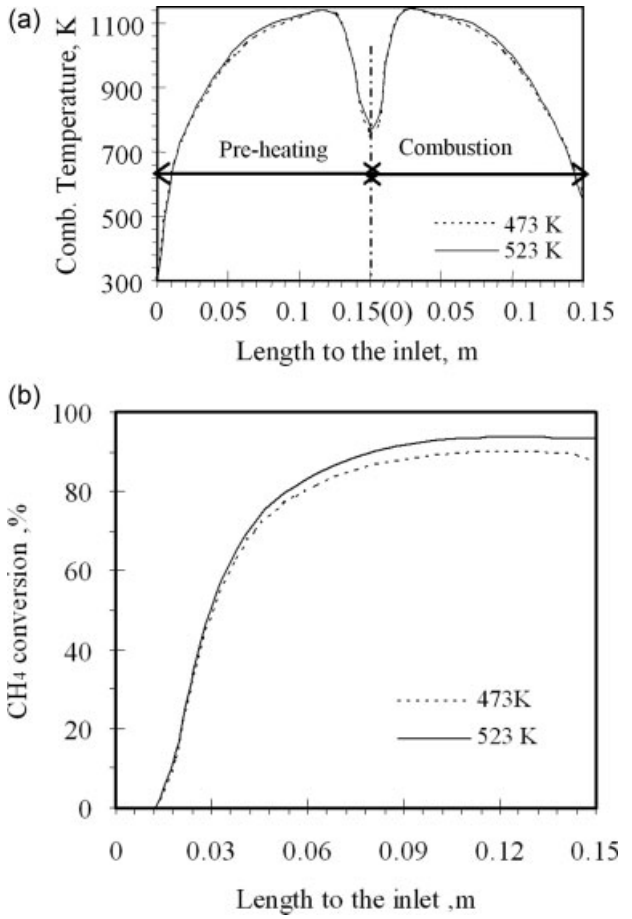

Figure 3. The profile of PHER for (a) the temperature in the combustion chamber with different inlet temperature and (b) methane steam conversion in the reforming chamber at t = 120 min.

difference of the two chambers is not more than 5 K when $l > 0.3$ m. In contrast to 250 K difference in temperature of outside wall and mean gas phase usually observed in the fixed-bed reformer, the plate reactor shows an efficient heat transfer performance. Furthermore, Figure 2c also shows the mole fraction distributions in the reforming channel. Before the first 0.03 m length of the reformer, remarkable changes of the reactant's concentration are found, which indicates that the reforming reactions are successfully aroused by methane combustion. The outlet CO-concentration reaches 13.2% and H_2-concentration is formed to 43% under this operational condition.

Figure 3 shows the performance of the PHER affected by different reforming inlet temperatures. It can be seen that, even the combustion inlet temperature is set at 298 K, the reforming reaction can be promoted when the reforming inlet temperature at 473 and 523 K. Figure 3a illustrates the temperature profiles in the preheating chamber and combustion chamber. In the preheating chamber, the feed gas temperature is heated from 298 K to 1100 K at 0.11 m to the inlet. It can be seen that, the inlet temperature of the reforming chamber do not make a significant temperature difference to

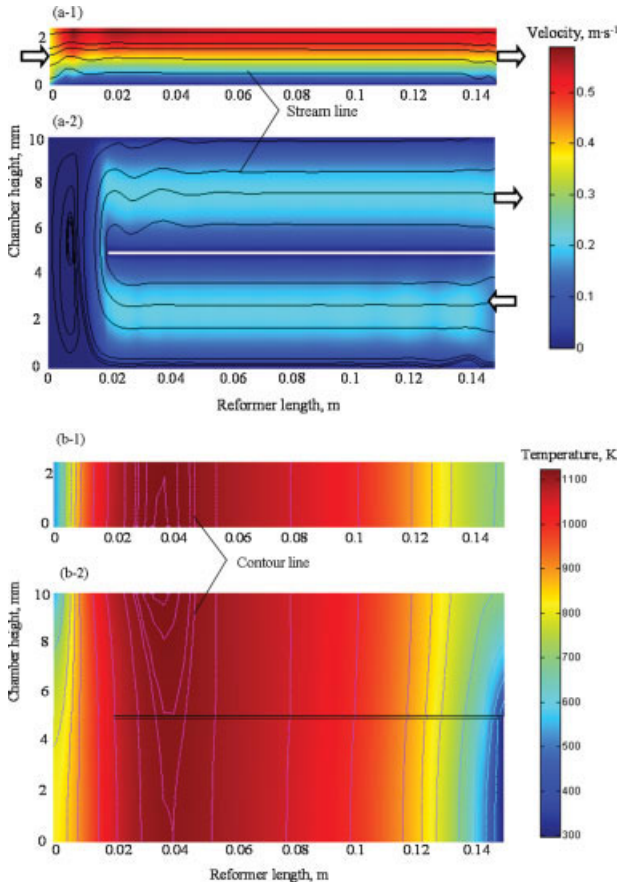

Figure 4. (a) Velocity field surface and stream line profiles in the PHER for (a-1) reforming chamber and (a-2) combustion + preheating chambers; (b) temperature distribution and contour profiles in the (b-1) reforming chamber and (b-2) combustion + preheating chambers.

[Color figure can be viewed in the online issue, which is available at www.interscience.wiley.com.]

the whole temperature distribution, which means that if the temperature of the inlet gas for the combustion chamber can be warmed beyond 740 K the combustion reaction can be successfully caused. Meanwhile, the results of CH_4 reforming conversion show that though the lower inlet temperature of the reforming chamber inevitably decreases the reaction performance of the reformer, and compared with the HER, the effects of inlet temperature are remarkably diminished.

Furthermore, to have a more detailed investigation on the heat transfer behavior in the PHER, the 2-D velocity and temperature distributions in each chamber by setting the inlet temperatures of reforming and preheating chamber with 523 K and 298 K separately are shown in Figure 4. In Figure 4a, the streamlines show the gas flow situation. As the Reynolds number is not more than 50 in all runs, the gas is found to be the laminar flow. Meanwhile, the vortexes are also detected in the left corner of the combustion + preheating chamber due to the redirection of the feed gas from the preheating chamber to the combustion chamber. Based on the flow states, the profiles of temperature in each chamber are displayed in Figure 4b. A hot spot is found at 0.035 m to the inlet of combustion chamber which shows a rapid temperature rise, indicating the combustion is aroused. Meanwhile, two temperature decrease phenomena are detected near the two sides of the reformer. On the left side of the reformer, the gas temperature shows a decrease profile because of the effect of the cold inlet temperature of reforming feed gas. However, even affected by the lower inlet temperature of reforming gas, the inlet temperature of the combustion chamber is maintained beyond 740 K, which ensures a prompt ignition of the combustion reaction. At the right side of the combustion chamber, the temperature is cooled down which is attributed to the endothermic reforming reactions, and the combustion reaction rate is getting smaller together with the effects of the cold inflow in the preheating chamber. Therefore, taking the huge endothermic character of the reforming side into account, the cocurrent flow in the combustion and reforming chambers is favorable, as the generated heat would not be sufficient to arouse the reforming reaction in the case of countercurrent flow directions.[10,21] Meanwhile, the outlet temperature of the reforming chamber is found to be nearly 673 K, which is very beneficial to the subsequent process without specially heat-exchange. Furthermore, it is noted that the transverse temperature differences along the chamber height are very small, which shows the plate reformer has a good heat transfer performance.

Figure 5 shows the profiles of the outlet CH_4 reforming conversion of each chamber affected by the chamber heights. For the HER, while setting the inlet temperature of each channel at 723 K, the conversions change slightly even as the channel height increases from 3 to 7 mm. It is assumed the wall-type reactor will offer stable thermal exchangeability, owing to the excellent conductive heat transfer of the catalyst.[22] Similar results were also reported by other simulation work.[14] Meanwhile, the constant profile of the conversion also suggests the possibility of reformer miniaturization. However, it is noted that for the PHER, the conversion slightly decreased when the chamber height is within the range of 3 to 4.5 mm, whereas the conversion shows a significant decrease profile when the chamber height is larger than 4.5 mm. To explain those phenomena, the gas/solid mass transfer limitations were investigated by the Damkohler number[23]:

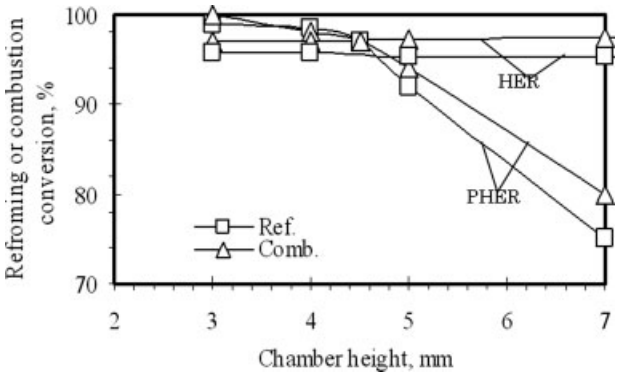

Figure 5. Effects of the chamber height on the performance of the reformers.

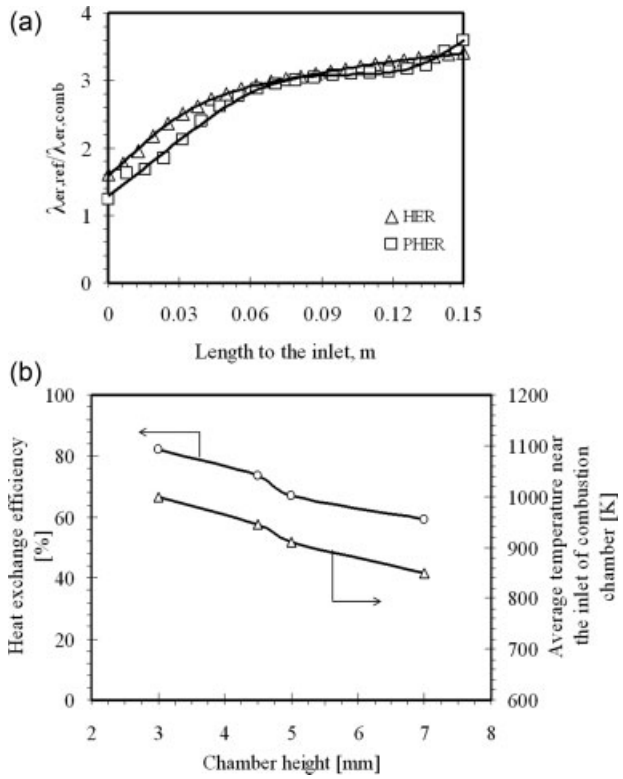

Figure 6. (a) Ratio of gas thermal conductivity between reforming and combustion chamber for PHER and HER with chamber height of 5 mm and (b) heat exchange efficiency and average temperature near the inlet of the combustion chamber functions of the chamber height for PHER.

$$\mathrm{Da} = \frac{w_1 d \delta_2 / \rho^{\mathrm{cat}}}{D_{\mathrm{r\ CH_4}} C_{\mathrm{CH_4}}} \tag{13}$$

where d represents the hydraulic diameter of the chamber and δ_2 means the thickness of the catalyst layer. It was found that Da < 0.01 under all the reaction conditions for HER and PHER. This indicates that the rate of gas/solid mass transfer in the chambers was always much greater than the rate of reaction, so that diffusion limitation can be safely neglected. Therefore, for HER, as the inlet temperatures of the combustion chamber are the same, the reforming conversion is stable even the chamber height increases. On the other hand, Figure 6a shows the profiles of ratio of the gas thermal conductivity between reforming and combustion chambers with a chamber height of 5 mm in case of HER and PHER. It can be found that the reforming gas's conductivity is near four times that of the combustion gas for the two reactors, which is attributed to the hydrogen existing in the reforming gas. As the high thermal conductivity of gas in reforming chamber ensures an excellent heat transfer, the heat transfer of the preheating and combustion chamber should be the reason why the reaction performance decreases with the chamber increasing. The heat exchange efficiency at different chamber height was shown in Figure 6b, which was calculated as:

$$\eta = \frac{(\bar{T}_{\mathrm{comb}} - T_{\mathrm{pre,out}})}{(\bar{T}_{\mathrm{ccomb}} - T_{\mathrm{pre,_{in}}})} \times 100\% \tag{14}$$

where $\bar{T}_{\mathrm{comb}}$ denotes the average temperature in the combustion channel. $T_{\mathrm{pre,_{in}}}$ and $T_{\mathrm{pre,_{out}}}$ mean the inlet and outlet temperature of the preheating chamber, respectively. It can be seen that, with the chamber height increasing, the heat exchange efficiency keeps decreasing. This implies that the heat transfer between the preheating and combustion chambers is getting worse, and consequently obtained a lower temperature profile when the gas flows from the preheating chamber into the combustion chamber as shown in Figure 6b. It directly affects the heat generation of the combustion reaction and leads to low reaction temperature of the reforming chamber. As the reactors are under reaction control, the temperature's decrease inevitably makes the reforming conversion lower.

Effects of electrically heating start-up strategy

One of the highlights of this study is to start up the reformer by EHAC. In our previous study, we have compared the difference of electrically internal heating and external heating methods and electrically heating start-up phenomena.[17,24] On the other hand, as the heat generated by the methane combustion reaction is supplied to the endothermic side to sustain the reforming reactions, the amount of the fuel is also an essential factor for the heat exchange system. In this study, the fuel ratio, ς, as defined as the ratio of the methane mass flow rates in the combustion and reforming chambers as shown in Eq. 15 were applied to simulate the necessary amount of the fuel.

$$\varsigma = G_{\mathrm{CH_4,comb.}} / G_{\mathrm{CH_4,ref.}} \tag{15}$$

where G denotes the mass flow rate. The operation steps were set at electrically heating the catalyst during the first 3 min to warm up the reactor and arousing the reactions, and then turning the power off. The process would be maintained with the generated combustion heat. To simulate a cold start situation, the initial temperature in the reformer was set at 298 K. Figure 7 shows the dynamic profiles of the outlet methane mole fraction and the hot-spot temperature in the reformer for PHER by setting ς from 0.12 to 0.2. With ς increasing, the methane mole fraction shows a decreasing profile, and when $\varsigma = 0.2$, the methane completely reacted. However, the increase of the fuel amount inevitably causes a higher combustion temperature, even causes temperature runaway. It can be seen that, when ς is less than 0.2, the hot-spot temperature is successfully controlled to nearly 1100 K, whereas when ς reaches 0.2, the hot-spot temperature increases greatly and approaches 2000 K, which is unfavorable for the catalyst's durability. On the other hand, it is also found that the methane mole fraction decreases dramatically in the first 3 min, which is attributed to the 3-min electrically heating which gives a prompt and huge heat supply. It can be seen that, the methane mole fraction returns to 0.11 after electrically heating has ended, which indicates the fuel amount is insufficient. Based on the results, it should be favorable that ς should be nearly 0.16.

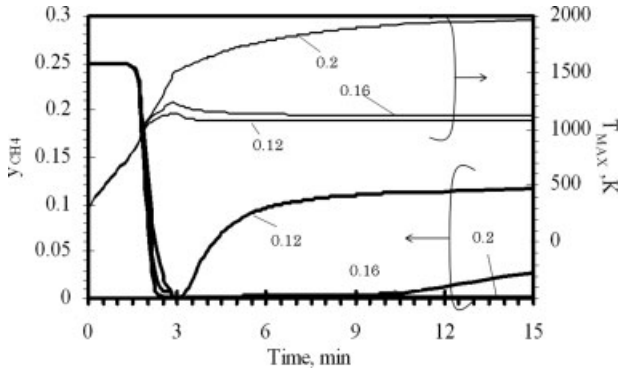

Figure 7. Effects of the fuel ratio on the reforming performance and heat point temperature for the PHER.

The numbers exhibited in the figures show fuel ratio, ς.

Figure 8a shows the transient average gas temperature profiles in the reforming chamber for the PHER when ς is 0.16. It can be seen that in the first 3 min, the temperature along the reforming chamber increased dramatically, and when the operation time reached 3 min, the highest temperature was nearly 1240 K, which implies the combustion reaction has been successfully ignited. It is noted that, when the power is off, the temperature decreases gradually till the temperature profiles reaches a steady state. It is because the additional input heat by electrically heating disturbs the reaction system's steady state; therefore, it is inevitable for it to take several minutes to reach a new steady state after the disturbance. Furthermore, it is also implied that if the electrical supply heat, q_{elec}, is so big that it will cause a big divergence from the steady state, after which will take a long time to return to the steady state. Figure 8b shows the transient temperature distribution in the combustion and preheating chambers. It can be seen that after 2 min, the gas in the preheating chamber is remarkably warmed up by the generated combustion heat. After 3-min electrically heating, the combustion reaction is completely aroused, and the preheating gas has successfully warmed up by the heat recovery. After 10 min, a distinctive temperature heat spot cannot be identified any longer, which indicates that after the disturbance of electrically heating, the combustion reaction becomes less severe. It also indicates that for the start-up process, the input heat plays an important role to control the combustion reaction's progress.

Figure 9 compared the start-up performance affected by q_{elec} of the two reformers. It can be seen that, the higher the q_{elec} is, the shorter the obtained start-up time. However, if the reformer is overheated, the phenomena of the temperature runaway can be observed. For the HER, as the inlet temperature is high enough to ignite a combustion reaction, the needed electrical heat is less than that for the PHER. As in the PHER, heat is efficiently recovered to warm up the cold inflow of the combustion gas, the outlet temperature of the PHER is no more than 680 K while that of the HER is more than 1000 K, which implies that for the HER's outgas, a cooling process is needed for the subsequent CO shift reaction process while that is not the case for the PHER.

Heat exchange system of the reforming process

The Japanese investigation committee for the stationary fuel cell system marketing strategies reported that fuel processor, including the reforming and heat exchange system, has taken up 12% of the total cost and 30–40% of the volume of the fuel cell system.[25] Therefore, to reduce the cost down and downsize the account, optimization of the heat exchange system of the fuel processor is urgent. Figure 10a shows the regular heat exchange system of the steam reforming process.[26] It can be seen that at least five heat exchangers are necessary for the fuel processor. The combustion gas must be preheated from 298 K to 573 K before conducted to the burner. And the high-temperature outlet gas of the reformer must be cooled for the following low-temperature CO shift reactor. Considering the results of PHER discussed earlier,

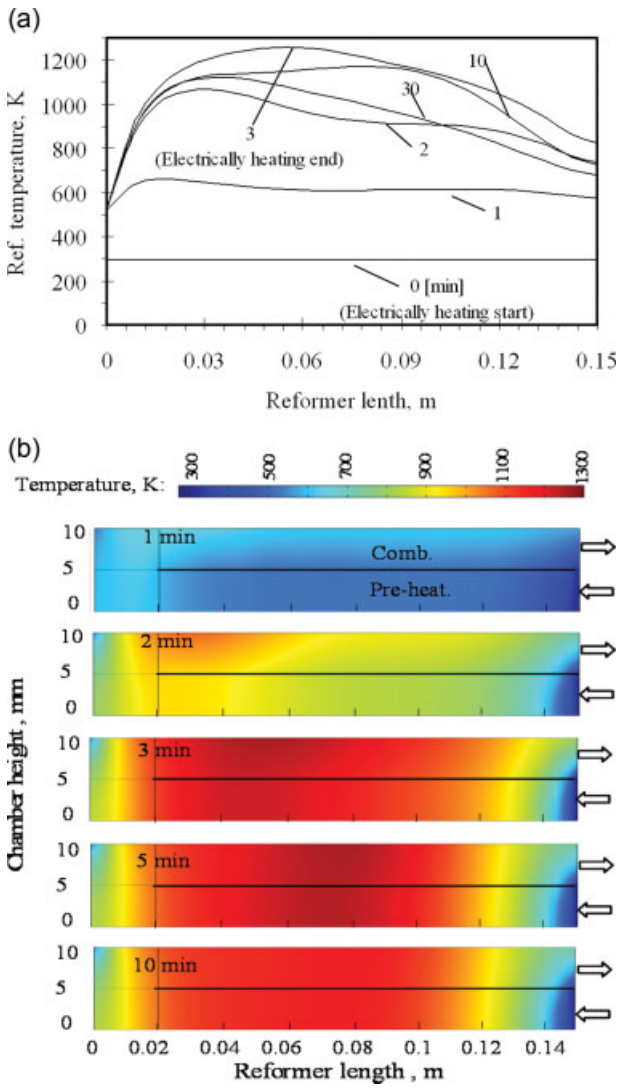

Figure 8. Transient profiles of the temperature distribution (a) in the reforming chamber and (b) in the combustion and preheating chamber with 3-min electrically heating.

[Color figure can be viewed in the online issue, which is available at www.interscience.wiley.com.]

the outlet temperature of the reforming chamber is nearly 680 K (as shown in Figure 6), which is suitable for the following low-temperature CO shift reaction. Furthermore, the inside heat exchange system makes it possible to conduct the combustion gas without any warming up (as shown in Figure 3). Therefore, a simplified heat exchange system by using the PHER is proposed in Figure 10b. Compared with the ordinary heat exchange system, 2/5th of the heat exchangers are omitted, which is very promising for issues of fuel cell system's cost and size. On the other hand, the integrated chambers can constitute a single unite of reformer, which was easy to be placed and scaled up to meet the needs of different class fuel cell system.

Conclusions

A compact PHER was numerically developed based on the ordinary HER coupled with just the reforming and combustion chambers. The simulation results revealed the possibility to start the reformer by conducting the combustion gas of 298 K by electrical heating through the catalyst at the beginning of the operation. Compared with the HER, the high heat exchange efficiency of PHER is promising to be utilized in the fuel processor systems to simplify the heat exchange system.

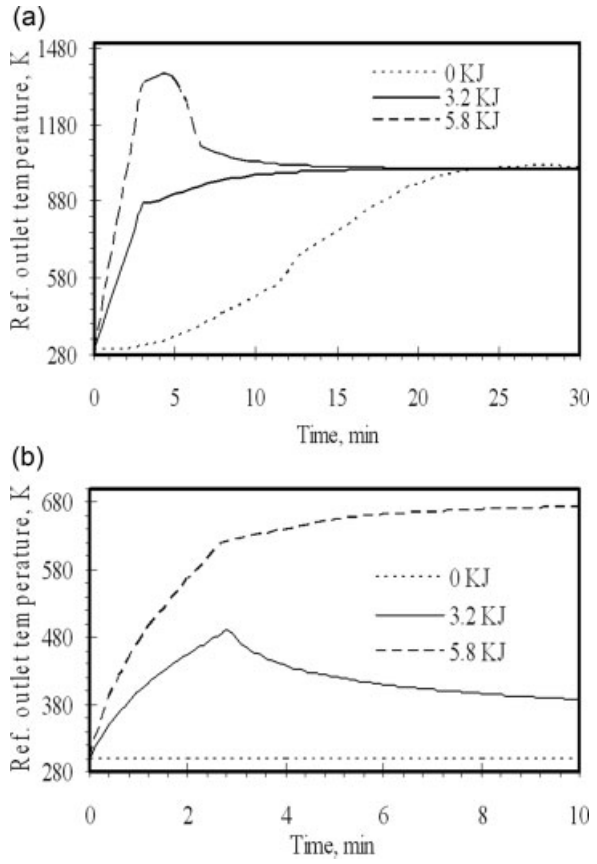

Figure 9. The start-up profile affected by different heat input (a) for the HER and (b) for the PHER.

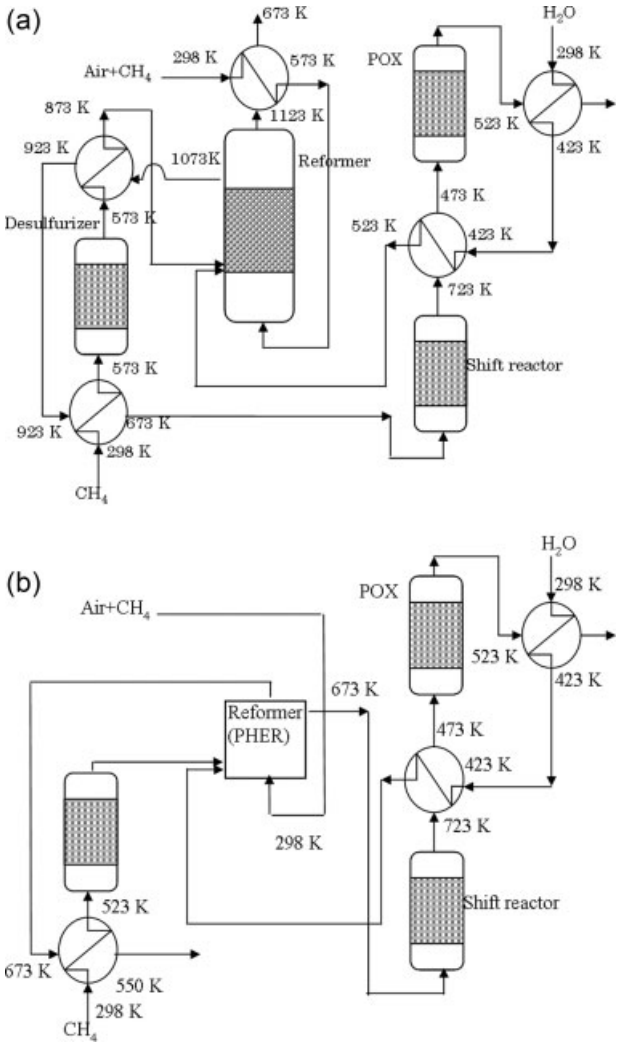

Figure 10. (a) Ordinary heat exchange system of the fuel processor[26]; (b) simplified heat exchange system of the fuel processor.

Notation

C_p = heat capacity, J kg^{-1} K^{-1}
C_{CH_4} = concentration of CH_4, mol m^{-3}
d = hydraulic diameter, m
Da = Damkohler number
D_{eff} = effective diffusion coefficient, m^2 s^{-1}
D_r = diffusion coefficient, m^2 s^{-1}
G = mass flow rate, kg s^{-1}
H = heat of reaction, J mol^{-1}
k = reaction rate constant
K = equilibrium constant
l = axial coordinate, m
L = reforming length, m
M = molecular weight, kg mol^{-1}
P = pressure, Pa
$q_{elec.}$ = input heat by electrically heating, J
r = transverse coordinate, m
R_p = catalyst pore radius, m
R_g = gas constant, J mol^{-1} K^{-1}
t = time, s or min
T = temperature, K
u = velocity, m s^{-1}

w = reaction rate, mol kg^{-1}_{cat} s^{-1}
y = mole fraction

Greek letters

δ = thickness, m
ε = catalyst porosity
ς = fuel ratio
λ_{er} = gas thermal conductivity, W m^{-1} K^{-1}
μ = viscosity, kg m^{-1} s^{-1}
ρ = density, kg m^{-3}
τ = catalyst tortuosity

Subscript and superscript

alloy = alloy layer
cat = catalyst
gas, g = gas phase
i = component of the reactions
in = inlet
j = reaction system (j = 1, reforming ; j = 2, combustion)
l = axial direction
m = reactions (m = 1 steam reforming reaction; m = 2 water shift reaction; m = 3 methane combustion reaction)
r = transverse direction

Literature Cited

1. Nagata Y, Tanka T, Arai Y. 1 kW fuel cell system for residential use. *Toshiba Rev*. 2001;56:19–24.
2. Echigo M, Tabata T. Simulation of the natural gas steam reforming process of PEFC systems. *J Chem Eng Japan*. 2004;37:723–730.
3. Van H. Methane steam reforming. *Catal Rev Sci Eng*. 1980;21:1–51.
4. Zanfir M, Gavriilidis A. Catalytic combustion assisted methane steam reforming in a catalytic plate reactor. *Chem Eng Sci*. 2003;58: 3947–3960.
5. Oohara H, Yamanaka Y, Kobayashi K, Fukuchi Y. Operation characteristics and results of the 5 kW PEFC co-generation system. *Ishikawajimaharima Technol Issue*. 2003;43:191–195.
6. Safonov MS, Fomin AA, Serdyukov SI, Nasonovskii IS, Voskresenskii NM, Granovskii MS. Mathematical model and performance tests of an experimental heat exchanger reactor with a sectional catalyst unit for benzene hydrogenation. *Teoreticheskie Osnovy Khimicheskoi Tekhnologii*. 1995;31:269–278. (Engl. trans.).
7. Bel'nov VK, Voskresenskii NM, Serdyukov SI, Karpov II, Barelko VV. Mathematical modeling of endothermic reactions in the catalyst unit with structured catalytic beds. *Chem Eng Sci*. 2003;58:1895–4901.
8. Guo Y, Kameyama H. Preparation of alumite support and preliminary activity investigation for NO removal in SCR-HC over alumite catalyst. *J Chem Eng Japan*. 2003;36:1470–1479.
9. Wang L, Vien VD, Suzuki K, Sakurai M, Kameyama H. Preparation of anodised aluminum catalysts by an electrolysis supporting method for VOC catalytic combustion. *J Chem Eng Japan*. 2005;38:106–112.
10. Zhang Q, Wang L, Sakurai M, Kitajima T, Nakaya M, Ootani T, Takahashi H, Kameyama H. Two-dimensional coaxial model for a cylinder methane steam reformer using a novel plate catalyst. *J Chem Eng Japan*. 2006;39:1172–1181.
11. Zhang Q, Koyama S, Iqbal A, Tran TP, Takahashi H, Kawate S, Kameyama H. Development of methane steam reformer for domestic fuel cell by using electro-thermal alumite catalyst. In the 10th APCChE Congress, 1P-08-024, Kitakyusyu, Japan, Oct. 2004.
12. Hunter JB, McGuire G. Method and apparatus for catalytic heat exchange. US Patent 4,214,867, 1980.
13. Reay DA. Catalytic combustion: current status and implications for energy efficiency in the process industries. *Heat Recovery Systs CHP*. 1993;13:83–390.
14. Fukuhara C, Igarashi A. Performance simulation of a wall-type reactor in which exothermic and endothermic reactions proceed simultaneously, comparing with that of a fixed-bed reactor. *Chem Eng Sci*. 2005;60:6824–6834.
15. Numaguchi T, Kikuchi K. Intrinsic kinetics and design simulation in a complex reaction network: steam-methane reforming. *Chem Eng Sci*. 1988;43:2295–2301.
16. Trimm DL, Lam CW. The combustion of methane on platinum-alumina fiber catalyst-I. Kinetics and mechanism. *Chem Eng Sci*. 1980;35:1405–1413.
17. Zhang Q, Sakurai MH, Kameyama H. Performance simulations of a compact plate methane steam reformer using electrically heated alumite catalyst. *J Chem Eng Japan*. 2007;40:487–496.
18. Cussler EL. *Diffusion: Mass Transfer in Fluid Systems*, 2nd ed. Cambridge: Cambridge University Press, 1997.
19. Groppi G, Tronconi E, Forzatti P. Mathematical modeling of catalytic combustors fuelled by gasified biomasses. *Catal Today*. 2000;59:151–162.
20. COMSOL. *COMSOL Multiphysics User's Guide*. Stockholm: COMSAOL AB, 2005.
21. Fukuhara C, Kobayashi S, Igarashi A. Simulations of dynamic performances of the plate-wall reactor. *Sekiyu Gakkaishi*. 1995;38:88–96.
22. Kameyama H. Heat transfer material with porous alumina layer. *Suiso Energy Shisutemu*. 1995;20:16–23.
23. Tronconi E, Groppi G. A study on the thermal behavior of structured plate-type catalysts with metallic supports for gas/solid exothermic reactions. *Chem Eng Sci*. 2000;55:6021–6036.
24. Zhang Q, Nakaya M, Ootani T, Takahashi H, Sakurai M, Kameyama H. Simulation and experimental analysis on the development of a co-axial cylindrical methane steam reformer using an electrically heated alumite catalyst. *Int J Hydrogen Energy*. 2007;32:3870–3879.
25. Polman EA, Der Kinderen JM, Thuis RMA. Novel compact steam reformer for fuel cells with heat generation by catalytic combustion augmented by induction heating. *Catal Today*. 1999;47:347–351.
26. Larminie J, Dicks A. *Fuel Cell System Explained*, *2nd ed*. England: Wiley, 2003.

Manuscript received Jan. 21, 2008, and revision received May 27, 2008.